Structural and optical properties of Ag-doped copper oxide thin films on polyethylene napthalate substrate prepared by low temperature microwave annealing

Sayantan Das and T. L. Alford

Citation: Journal of Applied Physics **113**, 244905 (2013); doi: 10.1063/1.4812584
View online: http://dx.doi.org/10.1063/1.4812584
View Table of Contents: http://scitation.aip.org/content/aip/journal/jap/113/24?ver=pdfcov
Published by the AIP Publishing

Structural and optical properties of Ag-doped copper oxide thin films on polyethylene napthalate substrate prepared by low temperature microwave annealing

Sayantan Das and T. L. Alford[a)]
Department of Chemistry and Biochemistry, Arizona State University, Tempe, Arizona 85287, USA and School for Engineering of Matter, Transport and Energy, Arizona State University, Tempe, Arizona 85287, USA

(Received 23 April 2013; accepted 14 June 2013; published online 27 June 2013)

Silver doped cupric oxide thin films are prepared on polyethylene naphthalate (flexible polymer) substrates. Thin films Ag-doped CuO are deposited on the substrate by co-sputtering followed by microwave assisted oxidation of the metal films. The low temperature tolerance of the polymer substrates led to the search for innovative low temperature processing techniques. Cupric oxide is a p-type semiconductor with an indirect band gap and is used as selective absorption layer solar cells. X-ray diffraction identifies the CuO phases. Rutherford backscattering spectrometry measurements confirm the stoichiometry of each copper oxide formed. The surface morphology is determined by atomic force microscopy. The microstructural properties such as crystallite size and the microstrain for (−111) and (111) planes are calculated and discussed. Incorporation of Ag led to the lowering of band gap in CuO. Consequently, it is determined that Ag addition has a strong effect on the structural, morphological, surface, and optical properties of CuO grown on flexible substrates by microwave annealing. Tauc's plot is used to determine the optical band gap of CuO and Ag doped CuO films. The values of the indirect and direct band gap for CuO are found to be 2.02 eV and 3.19 eV, respectively. © *2013 AIP Publishing LLC*. [http://dx.doi.org/10.1063/1.4812584]

I. INTRODUCTION

Transition metal oxides have gained considerable interest recently due to their potential application in solar cells,[1] displays,[2] sensors,[3] and supercapacitors.[4] Among them, copper oxides are nontoxic and the abundant availability of copper makes these oxides a cheap material available for many applications. Cupric oxide is a p-type semiconductor with an indirect band gap of 1.3–2.1 eV.[5] The application of CuO as selective absorbing layer has been reported because of its high solar absorption.[1] Herein, we report the preparation of Ag doped CuO thin films on flexible polymer substrates polyethylnapthalate (PEN).

The present work reports the use of microwave (MW) annealing to prepare transparent copper oxide coating on flexible polymer substrate, PEN. Polymer substrates offer added advantages over traditional rigid substrates like glass in terms of light weight and flexibility. However, fabrication of devices on flexible substrates is a challenge owing to the low temperature tolerance of the polymers. Previously, we have reported low temperature encapsulation of Ag films by copper oxides on Si using MW annealing technique.[6] Over the years, these electromagnetic waves have gained more and more importance recently in low temperature and quicker processing of materials with improved properties compared to conventional annealing techniques. Because of the photocatalytic properties of Ag/CuO nanocomposites reported by Wang *et al.*,[7] we also anticipate the use of Ag-doped CuO thin film coating on flexible solar panels with photocatalytic properties to decompose complex dirt particles.

II. EXPERIMENTAL DETAILS

Copper and Cu–Ag films were deposited on PEN and Si substrates by a DC magnetron sputtering system under vacuum using pure Cu and Ag targets (99.995% purity). The sputtering system was initially pumped down to 2×10^{-6} Torr and then Ar gas was introduced into the chamber. The depositions were done at room temperatures and at a pressure of 10 mTorr. This was followed by MW anneals inside a 2.45 GHz microwave cavity for 30 s. The temperature during the annealing process was measured using a Rayteck Compact MID pyrometer. The maximum temperature reached during the MW annealing process was 45 °C. The compositions of the as deposited and the MW annealed films were confirmed with Rutherford backscattering spectrometry (RBS) using a General Ionex Tandetron accelerator and analyzed using RUMP computer simulation program.[8] The structural properties of the as-deposited and annealed films were investigated by x-ray diffraction (XRD) using Bragg-Brentano configuration. X-ray photoelectron spectroscopy (XPS) studies were done using a VG-220IXL spectrometer with monochromatic Al $K\alpha$ radiation (1486.6 eV, line width = 0.8 eV). The pressure in the analyzing chamber was kept at a level of 10^{-9} Torr while recording the spectrum. The spectrometer had an energy resolution of 0.4 eV. All the binding energies were corrected with reference to C (1s) at 285.0 eV. Deconvolution of the spectrum was done using CASA software with an accuracy of 0.2 eV, after background subtraction with the Shirley method.[9] Optical transmittance of the films was measured

[a)]Author to whom correspondence should be addressed. Electronic mail: TA@asu.edu. Tel.: 001 480 965 7471

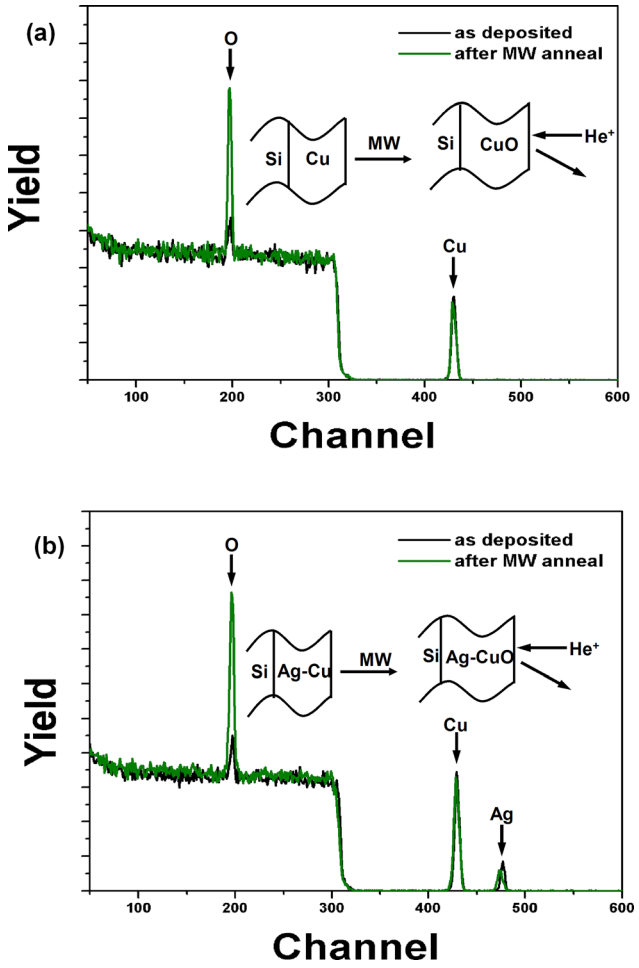

FIG. 1. RBS spectra obtained from (a) Cu and (b) Cu-Ag films before and after 30 s of MW annealing showing the growth of thin copper oxide layer. The spectra were obtained using a 3.05 MeV He^{++} beam and a scattering angle of 8°.

TABLE I. Ag content in CuO as determined by Rutherford backscattering spectrometry and RUMP computer simulation and surface roughness as determined by atomic force microscopy.

Sample	Ag content (at. %)	RMS roughness (nm)
CuO	0	1.01
Ag doped CuO	1	1.16
Ag doped CuO	3	0.591
Ag doped CuO	6	0.283

using an Ocean Optics double channel spectrometer (model DS200) in a wavelength range of 300–800 nm. Surface topography was evaluated using atomic force microscopy (AFM) in tapping mode.

III. RESULTS AND DISCUSSION

The deposition time for the films has been fixed for 1 min followed by a MW anneal for 30 s. The RBS results for CuO and 6 at. % Ag doped CuO thin films are shown in Figs. 1(a) and 1(b). RBS has been done on films deposited and processed on Si due to the ease of simulation on Si wafers. In case of as deposited samples, a small oxygen signal near channel 200 suggests the presence of oxygen at the surface of the films. After the MW anneal, the enhanced oxygen signal suggests the formation of an oxide layer. The RUMP simulation suggests that copper is completely oxidized after MW annealing. The shift in the Ag signal towards left in Fig. 1(b) after the MW anneal suggests that Ag diffuses from the surface towards the bulk CuO. The Ag content in the co-sputtered films obtained after RBS measurements and RUMP simulation has been detailed in Table I.

Figure 2 shows the surface topography of CuO and Ag-doped CuO films as measured by AFM and using $1 \times 1\ \mu m^2$

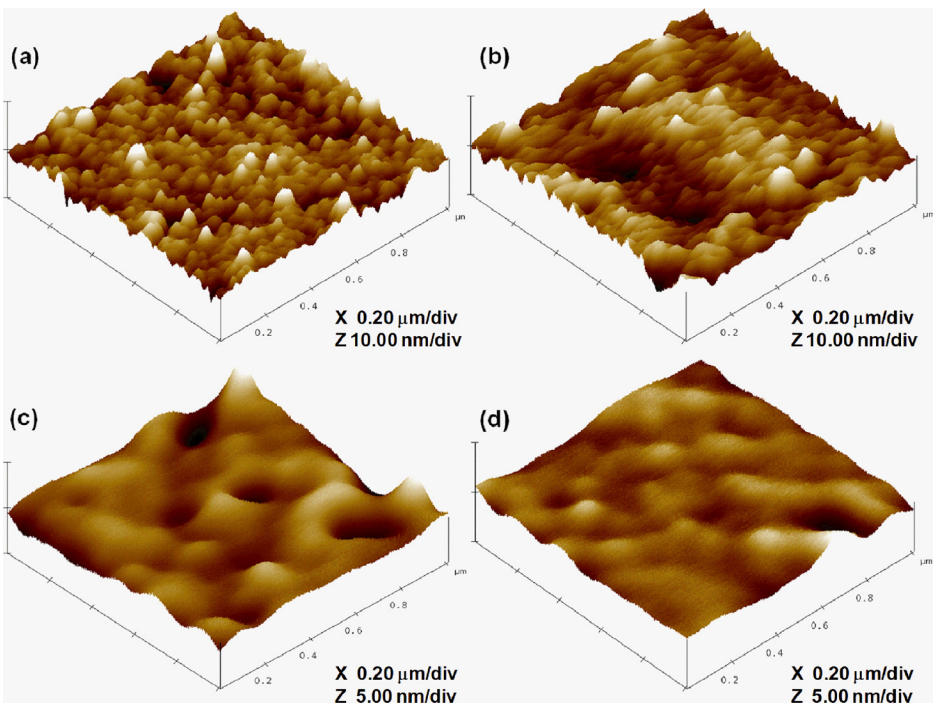

FIG. 2. AFM images of CuO thin films with: (a) 0 at. %, (b) 1 at. %, and (c) 3 at. % and (d) 6 at. % of Ag doping.

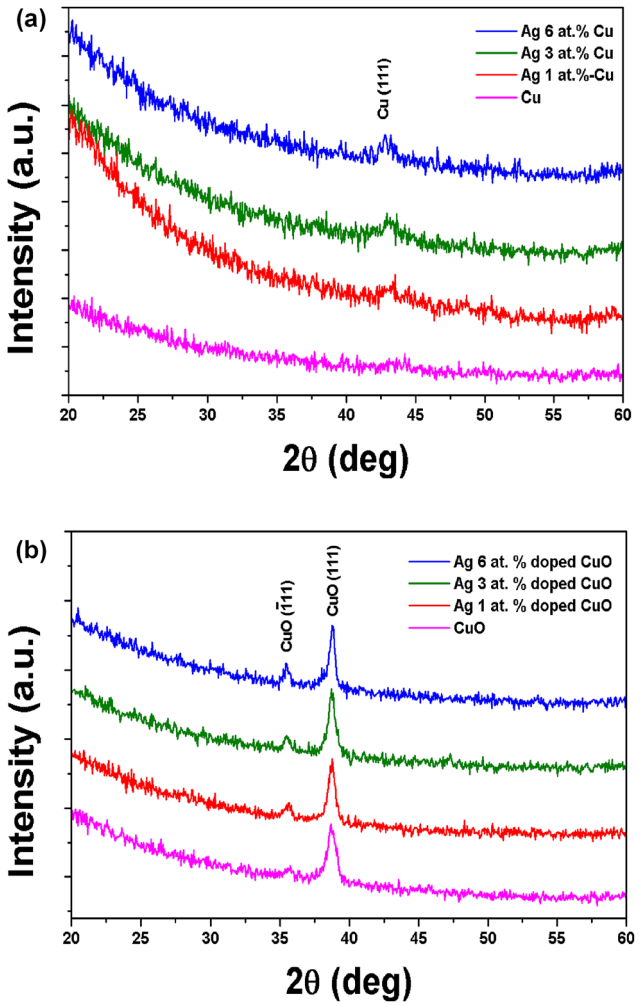

FIG. 3. XRD patterns showing (a) amorphous nature of the as-deposited films (b) growth of CuO after MW annealing.

scans. The surface roughness is found to be consistent over the sample size. It is also found that the undoped films have greater surface roughness than 3 and 6 at. % Ag-doped CuO films. The surface roughness is documented in Table I. As opposed to island formation in very thin Cu films, presence of increased amount of Ag in the alloy films produces continuous Cu films due to a grain boundary pinning effect.[10] After MW annealing, the undoped Cu films grow into CuO islands, whereas the Ag doped CuO films grows into uniform films. Thus, with increase in Ag content in the CuO matrix, the surface roughness is found to decrease.

XRD analysis using Cu $K\alpha$ radiation conveys the identification of phases present in the films. Figure 3 shows the XRD pattern of as deposited and MW annealed films indicating that the as-deposited films are amorphous and the MW annealed films are polycrystalline in nature. JCPDS card 89-5895 is used to identify the CuO peaks.[11] After MW annealing, the films show CuO peak at 35.5 and 38.7 (2θ) corresponding to the (−111) and (111) reflections of the monoclinic structure of cupric oxide (CuO). It is also observed that the films had preferential orientation in the [111] direction. The 2θ position of CuO (111) peak almost remains the same; however, a slight shift of the CuO (−111) peak is noticed in the Ag doped films towards lower

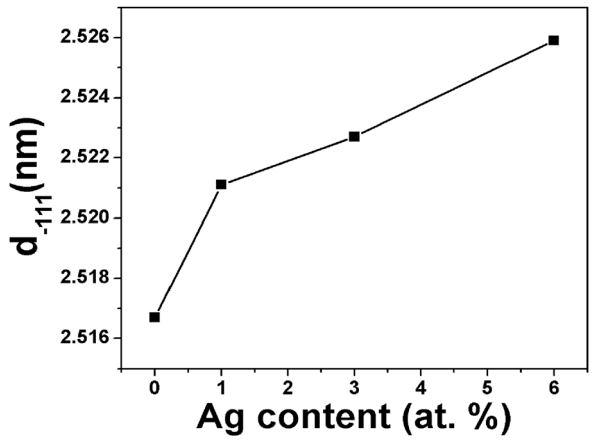

FIG. 4. Plot of CuO (−111) lattice spacing versus Ag content in the CuO films.

diffraction angle. It should be mentioned here that both CuO (−111) and (111) grains incorporate the Ag atoms; however, the symmetrical XRD scan is more sensitive to the lattice distortion in the (−111) grains that are parallel to the surface than the (111) grains in the same direction. Figure 4 shows the lattice spacing for (−111) planes as function of Ag content, which increases with the silver content. The full width at half maximum (FWHM) of the CuO (111) reflection peak decreases slightly with silver doping. However, the decrease in FWHM for the CuO (−111) peaks with increase in Ag content is higher. As such the variation in CuO (−111) grains is larger compared to the CuO (111) grains.

The crystallite size and microstrain are calculated for CuO films and tabulated in Table II. The crystallite size is calculated from the Debye-Scherer's formula using the FWHM in radians

$$D = \frac{0.9\lambda}{\beta \cos\theta}, \tag{1}$$

where D is the size of the crystalline domain and β is the FWHM. The decrease in the FWHM, β of the (−111) and (111) peak with Ag doping indicates the increase in grain size and also decrease in strain in the Ag doped CuO. The microstrain, ε in the CuO films are calculated from the well known Williamson-Hall relation[12]

$$\varepsilon = \frac{\beta \cos\theta - \frac{\lambda}{D}}{\sin\theta}. \tag{2}$$

The negative sign of the strain indicates that the strain is compressive. The crystallite size of CuO and doped CuO is

TABLE II. Microstructural properties extracted from X-ray diffraction data for Ag doped CuO films on PEN.

	Crystallite size, d (nm)		Microstrain, ε (%)	
Ag content (at. %)	(−111)	(111)	(−111)	(111)
0	10.7	11.6	−0.523	−0.447
1	11.5	13.7	−0.489	−0.379
3	14.5	15.1	−0.389	−0.343
6	20.8	17.7	−0.271	−0.293

dependent on factors such as defects and doping concentration. Moreover, in our case, the growth of CuO on flexible polymer substrates and the use of microwave annealing play a very important role in growth direction and rate. It has been hypothesized that during the deposition of Cu by sputtering, the lack of silver resulted in island formation; whereas, the presence of silver atoms led to the formation of a uniform layer of copper films by virtue of grain boundary pinning effect. After microwave annealing, Cu islands gets converted to CuO islands (in undoped films) and tends to produce more compressive strain than in continuous silver doped copper films, which gets oxidized to CuO films. The MW annealing also results in the presence of Ag at the CuO grain boundaries, which might increase the CuO-CuO grain boundary energy. This becomes the driving force for an increase in grain size by decreasing the grain boundary area of the film, thereby leading to increased crystallite size. Thus, the increase in the Ag content in CuO films results in reduction of compressive strain in the film and increase in crystallite size. It is our speculation that the Cu islands in undoped films are near-contiguous. Thus, upon oxidation, there is a net volume change taking place during the oxidation in the z-direction and radially. When adjacent oxidizing island continue to grow and becomes contiguous, there is inherent compressive strain. For the contiguous film as in Ag (6 at. %), the growth is in the z-direction and there is less compressive strain due to the large substrate size.

Figure 5 shows the variation of average crystallite size with roughness. It shows that as the average crystallite size increases as the surface roughness decreases. This is because increase in crystallite size reduces the grain boundaries due to grain growth and thus decreases the surface roughness. Previous thermal studies of Ag(Cu) alloy films using AFM and XRD to evaluate the texture and surface-morphology showed that the presence of Cu atoms in the silver alters the alloy's surface energy and surface diffusion.[13] This resulted in Ag and Ag(Cu) alloy having the very different surface morphologies and crystallographic texture after thermal annealing. The surface morphology was much smoother for the alloyed film when compared to the pure Ag film. In our case, the (111) texture of the Ag doped CuO was enhanced when compared to that of pure CuO films.

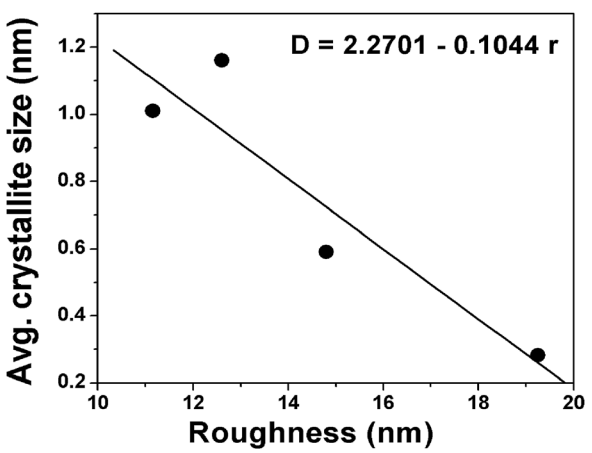

FIG. 5. Plot of average crystallite size versus roughness of the CuO films. The solid line represents the linear fitting of the experimental data.

The dataset has been fitted and found that roughness decreases linearly with increase in crystallite size. Herein, we propose an empirical relationship between crystallite size and roughness for CuO and Ag doped CuO films prepared on PEN by MW annealing

$$D = 2.2701 - 0.1044r. \quad (3)$$

From the above relation, the crystallite size can be roughly estimated from the surface roughness of CuO and doped CuO films on PEN prepared by MW annealing.

Figure 6(a) shows the Cu 2p XPS spectra for the as-deposited and the MW annealed Ag 6 at. % CuO sample. The peaks at 933 eV and 952.6 eV in the as-deposited sample are attributed to Cu $2p_{3/2}$ and Cu $2p_{1/2}$ of metallic Cu^0 state, respectively.[14] However, after the MW anneal, two distinct peaks are observed for Cu $2p_{3/2}$, which indicates the formation of both CuO and Cu_2O.[14] CuO was also characterized by the presence of shake-up satellite peaks at 9 eV higher than that of Cu $2p_{3/2}$ and Cu $2p_{1/2}$ peak.[15] The as-deposited samples showed small satellite peaks; however, the intensity of these satellite peaks increased after MW annealing showing the growth of CuO. Figure 6(b) showed that the broad Cu $2p_{3/2}$ peak, which had been deconvoluted into two peaks,

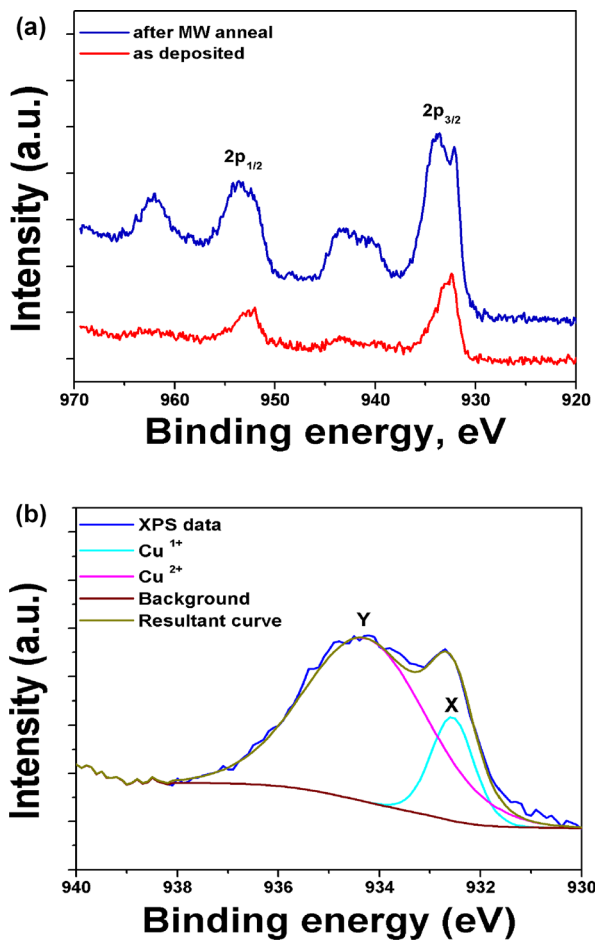

FIG. 6. XPS spectra showing Cu 2p peaks for (a) as deposited and MW annealed Ag 6 at. % CuO sample (b). The deconvoluted peaks of Cu^{2+} ($2p_{3/2}$) and Cu^{+}($2p_{3/2}$) with binding energy peaks at 934.3 eV and 932.5 eV, respectively.

marked as X and Y peaks. The X and Y peaks are ascribed to Cu_2O and CuO, respectively. The binding energy and FWHM of Cu_2O for the MW annealed samples are 932.5 eV and 1 eV, respectively. Whereas, the binding energy and FWHM of CuO for the MW annealed samples are 934.3 eV and 2.85 eV, respectively. Based on the areas of peak fit as shown in Fig. 6(b), the Cu(II):Cu(I) ratio is found out to be 4.5:1. Ag displayed a $3d_{5/2}$ peak at 368.5 eV (figure not shown) for both as-deposited and MW annealed samples corresponding to silver in zero oxidation state.

Copper oxidizes in preference to silver due to the higher oxygen affinity of copper, as is evidenced by the free energy calculations using FACTSAGE 5.4.1 thermochemical software and databases which is shown below[16]

$$\mathrm{Cu\,(s)} + \frac{1}{2}\mathrm{O_2\,(g)} \xrightarrow{\mathrm{MW}} \mathrm{CuO\,(s)},\ \Delta G_{rxn} = -126.5\,\mathrm{kJ/mol}. \tag{4}$$

An alternative mechanism suggests Ag_2O *in situ* oxidizes Cu to Cu_2O and itself gets reduced to metallic Ag. Thus, Ag_2O might have acted as a catalyst for low temperature oxidation of Cu

$$2\mathrm{Ag\,(s)} + \frac{1}{2}\mathrm{O_2\,(g)} \xrightarrow{\mathrm{MW}} \mathrm{Ag_2O\,(s)},\ \Delta G_{rxn} = -9.5\,\mathrm{kJ/mol}, \tag{5}$$

$$\mathrm{Ag_2O\,(s)} + \mathrm{Cu\,(s)} \xrightarrow{\mathrm{MW}} \mathrm{CuO\,(s)} + 2\mathrm{Ag\,(s)},\quad \Delta G_{rxn} = -412.2\,\mathrm{kJ/mol}. \tag{6}$$

Figure 7 shows the transmission spectra of the copper oxide films on PEN. It indicates that all the CuO films on PEN are opaque for wavelengths below 380 nm. The maximum transmittance of ~80% is observed around 600 nm for undoped CuO films. It is also noted that with the increase in the Ag concentration the transmittance decreased. Considering the application of these films in transparent solar panel, the average transmittance of these films has to be determined. The following equation is used to determine the average transmittance:

$$T_{av} = \frac{\int T(\lambda)V(\lambda)d\lambda}{\int V(\lambda)d\lambda}, \tag{7}$$

where $T(\lambda)$ is the transmittance and $V(\lambda)$ is the photopic luminous efficiency function defining the standard observer for photometry. In the blue part of the visible spectrum, the transmittance of the films decreases as the amount of silver increases. In case of noble metals like silver, the transmittance in the blue region is determined by the absorption of light due to electronic transitions between occupied d states and unoccupied hybridized *sp* states above the Fermi level.[17] With an increase in the silver content, the probability of interband electronic excitation increases and hence the greater drop in the transmittance occurs. In the red region, the transmittance of the films is governed by the reflectivity of silver, hence lower transmittance with increase in Ag content.[18]

The absorption coefficient were determined by transmission (T) and reflectance (R) data by using the following equation:

$$T - R = \exp(-\alpha t), \tag{8}$$

where t is the film thickness and α is the absorption coefficient. The bandgap (E_g) of the material can be deduced from the relation

$$(\alpha h\nu)^n \propto (h\nu - E_g), \tag{9}$$

where $h\nu$ is the incident photo energy and the exponent n depends on the type of transition, n = 2 and n = 1/2 for direct and indirect transition, respectively. Extrapolation of the linear portion of the curve to the energy intercept yields bandgap value of the materials. Figure 8 illustrates an excellent straight line fit and an abrupt increase in the absorbance, a characteristic feature of a well defined direct band gap. The interception generates a direct band gap, $E_{gd} \sim 3.19$ eV and 2.95 eV for CuO and Ag (6 at. %) doped CuO, respectively. Replotting the absorption coefficient data using Eq. (8) and n = 1/2 in Fig. 9 yields indirect bandgaps, $E_{gi} \sim 2.02$ eV and 1.89 eV for CuO and Ag (6 at. %) doped CuO, respectively.

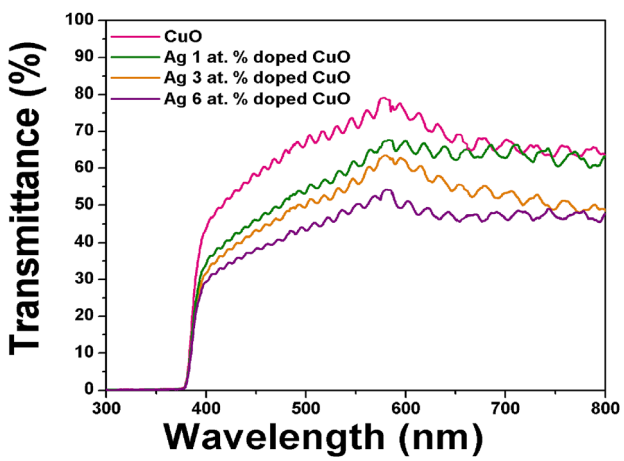

FIG. 7. Comparison of the transmission spectra of CuO films with different Ag contents.

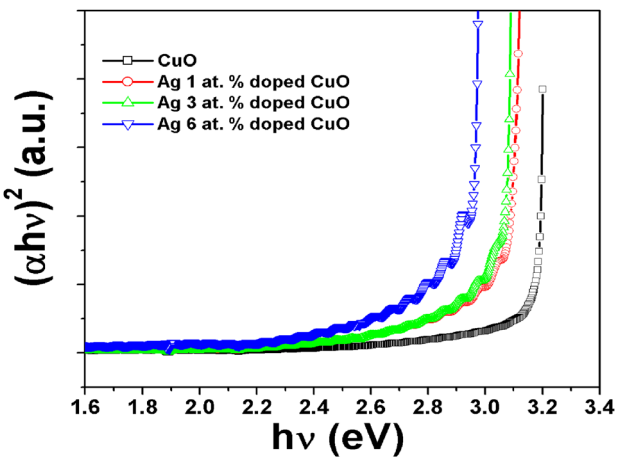

FIG. 8. Tauc's plot to estimate the direct band gap of CuO and Ag doped CuO.

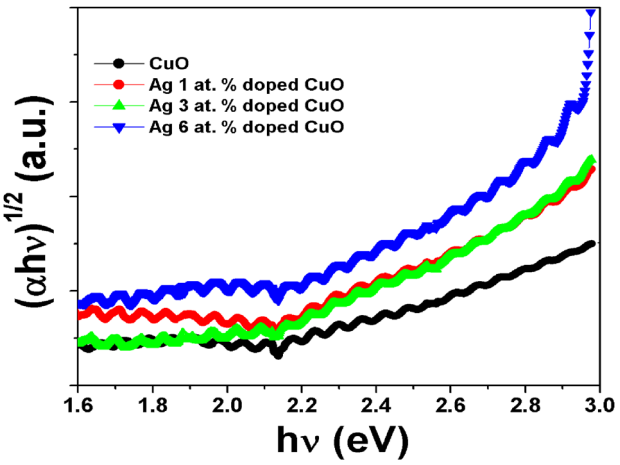

FIG. 9. Tauc's plot to estimate the indirect band gap of CuO and Ag doped CuO.

IV. CONCLUSIONS

It has been demonstrated that CuO thin films on PEN can be prepared by oxidation of pure copper to CuO using microwave radiation. This facile approach allows for low temperature, faster and controllable growth of metal oxide films on polymer substrates. XRD results show the formation of CuO (111) and (−111) peaks after MW anneals. XPS results confirm the formation of CuO after the MW anneal. The Ag doping led to the growth of smooth and uncracked films; however, the transparency is reduced with increased silver content. The transparent Ag doped CuO may offer potential applications in areas of photocatalysis, electronics, and optics.

ACKNOWLEDGMENTS

This work was partially supported by National Science Foundation (C. Ying, DMR-0902277) to whom the authors are greatly indebted.

[1]T. Maruyama, Sol. Energy Mater. Sol. Cells **56**, 85 (1998).
[2]G. Li, N. M. Dimitrijevic, L. Chen, T. Rajh, and K. A. Gray, J. Phys. Chem. C **112**, 19040 (2008).
[3]P. Peng, H. Huang, A. Hu, A. P. Garlich, and Y. N. Zhou, J. Mater. Chem. **22**, 15495 (2012).
[4]J. Huang, H. Wu, D. Cao, and G. Wang, Electrochim. Acta **75**, 208 (2012).
[5]F. Marabelli, G. B. Parravicini, and F. Salghettidrioli, Phys. Rev. B: Condens. Matter **52**, 1433 (1995).
[6]S. Das and T. L. Alford, Mater. Lett. **89**, 163 (2012).
[7]L. S. Wang, J. C. Deng, F. Yang, and T. Chen, Mater. Chem. Phys. **108**, 165 (2008).
[8]L. R. Doolittle, Nucl. Instrum. Methods Phys Res B **9**, 344 (1985).
[9]J. D. A. Shirley, Phys. Rev. B **5**, 4709 (1972).
[10]K. Barmak, A. Gungor, A. D. Rollett, C. Cabral, Jr., and J. M. E. Harper, Mater. Sci. Semicond. Process **6**, 175 (2003).
[11]V. Massarotti, D. Capsoni, M. Bini, A. Altomare, and A. G. G. Moliterni, Z. Kristallogr. **213**, 259 (1998).
[12]P. Goel and K. L. Yadav, J. Mater. Sci. **42**, 3928 (2007).
[13]H. Han, Y. Zoo, J. W. Mayer, and T. L. Alford, J. Appl. Phys. **102**, 036101 (2007).
[14]C. D. Wagner, W. M. Riggs, L. E. Davis, and J. F. Moulder, *Handbook of X-Ray Photoelectron Spectroscopy* (Perkin Elmer, Minnesota, 1978), pp. 82–83.
[15]S. Y. Lee, N. Mettlach, N. Nguyen, Y. M. Sun, and J. M. White, Appl. Surf. Sci. **206**, 102 (2003).
[16]C. W. Bale, P. Chartrand, S. A. Degterov, G. Eriksson, K. Hack, R. B. Mahfoud, J. Melancon, A. D. Pelton, and S. Petersen, CALPHAD: Comput. Coupling Phase Diagrams Thermochem. **26**, 189 (2002).
[17]J. H. Simmons and K. S. Potter, *Optical Materials* (Academic, San Diego, 2000).
[18]A. Indluru and T. L. Alford, J. Appl. Phys. **105**, 123528 (2009).